Rietbroek, R., Fritsche, M., Dahle, C., Brunnabend, S.-E., Kusche, J., Behnisch, M., Flechtner, F., Schröter, J., Dietrich, R. (2014): Can GPS-Derived Surface Loading Bridge a GRACE Mission Gap? - *Surveys in Geophysics*, *35*, 6, p. 1267-1283.

DOI: http://doi.org/10.1007/s10712-013-9276-5

Surveys in Geophysics manuscript No.
(will be inserted by the editor)

Can GPS derived surface loading bridge a GRACE mission gap?

Roelof Rietbroek · Mathias Fritsche · Christoph Dahle · Sandra-Esther Brunnabend · Madlen Behnisch · Jürgen Kusche · Frank Flechtner · Jens Schröter · Reinhard Dietrich

Received: date / Accepted: date

Abstract We investigated two 'gap-filler' methods based on GPS-derived low degree surface loading variations (GPS-I and GPS-C), and a more simple method (REF-S) which extends a seasonal harmonic variation into the expected GRACE mission gap. We simulated two mission gaps in a reference solution (REF), which is derived from a joint inversion of GRACE (RL05) data, GPS-derived surface loading and simulated ocean bottom pressure. The GPS-I and GPS-C methods both have a new type of constraint applied to mitigate the lack of GPS station network coverage over the ocean. To obtain the GPS-C solution, the GPS-I method is adjusted such that it fits the reference solution better in a 1.5 year overlapping period outside of the gap.

As can be expected, the GPS-I & GPS-C solutions contain larger errors compared to the reference solution, which is heavily constrained by GRACE. Within the simulated gaps, the GPS-C solution generally fits the reference solution better compared to the GPS-I method, both in terms of spherical harmonic loading coefficients and in terms of selected basin-averaged hydrological mass variations. Depending on the basin, the rms-error of the water storage variations (scaled for

R. Rietbroek, J. Kusche
Chair of Astronomical, Mathematical and Physical Geodesy, Nussallee 17, 53115, Bonn, Germany
Tel.: +49(0)22873-3577
E-mail: roelof@geod.uni-bonn.de

M. Fritsche, R. Dietrich
Institute for Planetary Geodesy, Dresden, Germany

C. Dahle, F. Flechtner
GFZ German Research Centre for Geosciences, Potsdam, Germany

S.-E. Brunnabend
Institute for Marine and Atmospheric research Utrecht, the Netherlands

J. Schröter, M. Behnisch
Alfred Wegener Institute, Bremerhaven, Germany

leakage effects), range between 1.6 cm (Yukon) and 15.3 cm (Orinoco). In terms of noise level, the seasonal gap-filler method (REF-S) even outperforms the GPS-I and GPS-C methods, which are still affected by spatial aliasing problems. However, it must be noted, that the REF-S method cannot be used beyond the study of simple harmonic seasonal variations.

Keywords Surface loading · GPS · GRACE · Basin averages · Mission gap

1 Introduction

The twin-satellite, NASA/DLR Gravity Recovery and Climate Experiment (GRACE) mission has changed the way we perceive the ongoing redistribution of mass within the Earth system. GRACE measures tiny changes in distance between two spacecraft resulting from static and time-variable irregularities of the Earth's gravity field. Its data products, usually provided in form of monthly spherical harmonic models of the gravity field, have enabled scientists to quantify cryospheric ice mass loss (Rignot et al 2011), ocean mass change (Chambers and Schröter 2011), or variability in terrestrial water storage (Tapley et al 2004; Schmidt et al 2008). More recently, GRACE data is increasingly used in assimilation schemes of ocean and hydrological models (Köhl et al 2012; Zaitchik et al 2008; Eicker et al 2014).

A follow-on mission for GRACE (GRACE-FO) is well on its way, with a launch date anticipated for August 2017 (Flechtner et al 2013). GRACE-FO will be equipped with a GRACE-heritage K-band ranging system but will carry, in addition, a Laser Ranging Interferometer (LRI, Sheard et al 2012). It is thus expected that GRACE-FO derived gravity field models will be at least as precise as GRACE-derived models, while, when the LRI is enabled, models with improved spatial and temporal resolution may be obtained (Flechtner et al 2013). However, the GRACE spacecraft are currently operating beyond their design lifetime of five years and signs of the ageing power system become apparent. Already since the beginning of 2011, once in 161 days (when the orbital plane is directed towards the Sun), three to four weeks of power saving mode must be scheduled which results in a loss of accelerometer and/or K-band ranging data. Although careful planning of the mission operation team minimizes the amount and length of the data gaps, a loss of data cannot be avoided without imposing unacceptable risk. Thus, depending on the GRACE lifetime and the actual GRACE-FO launch, there may be a gap of a year or longer between both missions.

The question whether we can find some way to 'bridge' either short gaps (of about several months) in GRACE mass change time series, or a longer, possibly multi-year gap occuring between GRACE and GRACE-FO, using measured geodetic data, is thus of immediate concern. Obviously, there is no silver bullet when one aims at substituting the micrometer-precise GRACE ranging measurements by any other space-geodetic technique. Any alternative approach will inevitably result in a serious loss in spatial and/or temporal resolution, when compared to GRACE. Its use in science applications may be limited and it needs to be investigated on a case-by-case basis. Notwithstanding this caveat, several approaches have been suggested in order to substitute GRACE results for continuing ice loss,

ocean mass and sea level separation, and large-scale hydrologic storage time series. These approaches include:

- combining satellite laser ranging (SLR) results, which provide the time variability of the very low-degree gravity harmonics for some 30 years now, with predefined mass change pattern whose derivation most probably involves analysing GRACE time series (e.g. GRACE-derived empirical orthogonal functions, Pilinski and Nerem 2011).
- using absolute and relative GNSS tracking to and between low-flying orbiters equipped with accelerometers, like the SWARM satellite constellation, in order to derive the low-degree time variable field up to degree 6 or so (Wang et al 2012); using GNSS tracking on GRACE A and/or B once the K-band ranging system would no longer being operational is along the same line of reasoning.
- using the technique known as loading inversion, where GNSS-measured, global network deformations are inverted into low-degree load distribution, possibly together with complementary information (Blewitt et al 2001).

In this contribution, we will focus on the last option. In this sense, our study extends previous work (Kusche and Schrama 2005; Wu et al 2006; Rietbroek et al 2009, 2012b) on combining GRACE and the loading inversion approach.

The surface loading inversion approach has been pioneered by Blewitt et al (2001); Wu et al (2006). It is based on the observation that redistributing mass near the Earth's surface does not only cause time variability in the gravity field, but also deforms the crust to an extent visible in large-scale permanent GNSS networks. When non-loading effects can be carefully reduced, this deformation may be inverted into spherical harmonics of surface mass. While early studies had focused on the retrieval of degree-1 loading, which remains unobserved by GRACE, more recent work has been devoted to reconciling differences between GRACE- derived mass redistribution at higher resolution and network-derived deformations. Results by Collilieux et al (2011); Rietbroek et al (2012b), demonstrate the impact of using reprocessed GPS observations, owing to improvements in GPS radiation pressure modelling, phase center modelling, and the consideration of higher-order ionospheric terms.

Here, we adapt the inversion scheme of Rietbroek et al (2009, 2012b). Surface loading variations are parameterized through a spherical harmonic expansion up to maximum degree and order 30, and are estimated in a weighted least squares approach involving GPS solutions from a recent reprocessing project provided by the TU Dresden, GRACE normal equations from GFZ, and simulated ocean bottom pressure derived from AWI's Finite-Element Sea-Ice Ocean Model (FESOM). The data characteristic are elaborated upon in Sec. 2. The resulting normal equation systems are processed in weekly batches, which are aligned to the GPS weeks. The results in this paper are additionally smoothed by rigorously stacking 5 weekly systems, in a running mean sense.

In order to investigate the potential impact of a mission gap, we proceed as follows. The results from the joint inversion are used as a reference dataset, against which the gap-filler solutions can be tested. We then simulate two data gaps within the reference solution, and additionally construct three types of gap-filler solutions.

The first gap-filler solution (GPS-I) is constructed by inverting the GPS data, which is additionally constrained over the ocean by a new type of regularization (described in Sec. 3.2). Alternatively, we compute a constrained GPS solution (GPS-C) which is additionally adjusted by applying correction parameters to the GPS data. These correction parameters (biases, trend and a seasonal harmonic) are estimated by adjusting the GPS network solution to the reference solution in an overlapping period outside the gap. For comparison, we also construct a third gap-filler solution by simply using a seasonal fit obtained from the reference solution (REF-S). For consistency, the data flowing in this fit originate from the same overlapping intervals as used above. Due to the limited coverage of the GPS stations we limit the maximum truncation degree of the spherical harmonic coefficients of the gap-filler solutions to 10.

2 Data

2.1 GPS Network Deformations

Data from a global network of 316 GPS stations are assembled into weekly unconstrained normal equation systems. A long term secular station position model (coordinates and velocities) has been estimated and is consequently removed a priori. In the same procedure, station discontinuities have been estimated and removed as well. In addition to our previous work, a priori surface loading has been accounted for by removing the same high frequency ocean and atmospheric dealiasing product, which is used in the GRACE processing. Although the effect is small, the station deformations associated with the ocean pole tide (Desai 2002) have been removed, such that the GPS systems are consistent with the GRACE processing. For consistency, and to mitigate the orientation rank defect of the unsolved GPS systems, the earth orientation parameters are fixed to values as used in the GRACE processing. Furthermore, the precise orbit determination of the GPS-satellites depend on arcs which are made as long as possible (reaching up to 7 days). The orbit parameters are reduced from the normal equation systems, which means that the parameters are implicitly solved but not part of the explicit parameter space anymore (e.g. Kusche 2003). Additional GPS processing standards, such as tidal corrections, higher-order ionospheric effects, and solar radiation pressure corrections, conform the description of Steigenberger et al (2006) and Fritsche et al (2005).

In a screening process, data from 12 stations, having less than a year's worth of data, have been excluded from all inversions.

The GPS satellites orbit the center of mass of the Earth system (CM), whereas the origin of the GPS station network (CN) approximates the center of surface figure (CF). This makes the GPS observation system sensitive to variations in the offset of the CM from the CN (see for example Wu et al 2012). In the normal equation systems, the station coordinates are expressed relative to the center of mass of the Earth system. We use the CM as the reference origin as it is a natural choice for space-borne observation systems. Furthermore, the CM itself is independent of the network geometry of the GPS stations, which may fluctuate over time.

2.2 GRACE Gravimetry

In this study, we use the GFZ GRACE data processed according to the release 05 processing standards (Dahle et al 2013). Similar to the GPS deformations, the data is provided in the form of weekly normal equation systems. This allows us to fully exploit the error-covariance information, and the solving step can be postponed until all data have been combined. In contrast to our earlier work, the errors have not been calibrated by a degree-wise factor, but a global weight is computed using Variance Component Estimation (VCE, see Sec. 3.1).

2.3 Simulated Ocean Bottom Pressure

Simulated ocean bottom pressure is computed by the Finite Element Sea-Ice Model (FESOM, Timmermann et al 2009). The model is based on the primitive equations and is forced by ECWMF fields (e.g. wind stress and pressure). Compared to the results of Rietbroek et al (2012b) a new heterogeneous horizontal discretization is implemented on a finite element mesh which varies significantly in size from 20 km (coastal regions/equator) to 150 km (open ocean).

When combining the ocean model data with geodetic observations, an estimate of the model's error-covariance is required. We obtain the error from the difference between two model runs, forced with different atmospheric datasets (ECMWF versus NCEP). From the time varying difference we first compute the median per finite element node. The absolute value of this median value is then taken as its representative error and is plotted in Fig. 1 (left). Off-diagonal error-covariances are not considered in this study. It is tempting to use these errors directly in the inversion. However, the sheer amount of nodes in regions with a finely resolved mesh would result in a grossly overweighted model in the joint inversion. For that reason, we also reweight the model error by its cluster area (this amounts to one-third of the surrounding triangle areas). In summary, the adopted error for each node, σP_i, is computed from the difference of the model runs, ΔP_i, as follows:

$$\sigma P_i = \sqrt{\frac{A_{med}}{A_i}}\,\mathrm{med}\left(|\Delta P_i(t_0 \cdots t_n)|\right) \tag{1}$$

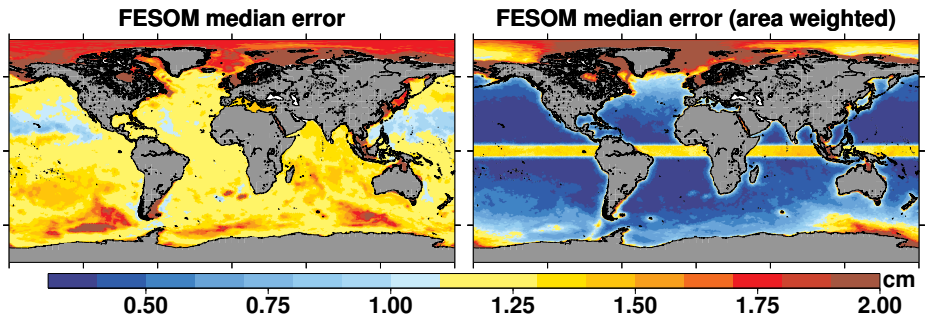

Fig. 1 Left: Median error (absolute value) of the FESOM model. Right: Area weighted median error (absolute value).

As can be seen, the cluster area, A_i is normalized by the median cluster area of the model A_{med}, which amounts to $1990\,\mathrm{km}^2$. The area-weighted error is plotted in Fig. 1 (right).

3 Surface Loading Retrieval

The three observables: ocean bottom pressure, potential changes and station deformations, can all be linearly linked to the unknown surface load. The observation equations have been extensively described in Rietbroek et al (2012b), but we repeat them here for completeness.
Firstly, the quantity of interest, $T(\theta,\lambda)$, expressed in an equivalent water height loading the Earth's surface, is written as a truncated expansion of spherical harmonic coefficients, T_{nm}:

$$T(\theta,\lambda) = a\sum_{n=0}^{N}\sum_{n=-m}^{n} T_{nm}\bar{Y}_{nm}(\theta,\lambda) \tag{2}$$

Where a denotes the mean Earth radius, and $\bar{Y}_{nm}$ are the 4π normalized (real) spherical harmonic base functions.

The relation between the (residual) Stokes coefficients, $\delta\Phi_{nm}$, from GRACE and the surface load are can be written as (see for example Wahr et al 1998):

$$\delta\Phi_{nm} = \frac{3\rho_w(1+k'_n)}{\rho_e(2n+1)}T_{nm} + \epsilon_{\Phi}, \quad n \geq 1 \tag{3}$$

Here, the density of water and the mean density of the Earth are denoted by ρ_w and ρ_e respectively. The load Love numbers, indicated by the symbol k'_n are derived from the PREM model (Dziewonski 1981). The error of the Stokes coefficients is denoted by, ϵ_{Φ}. The potential field of GRACE is described relative to the center of mass of the Earth system (CM). This implies that the terms with the degree 1 load Love number obey $(1+k_1^{'CM}) = 0$ (Blewitt 2003). Consequently, the inverse problem exhibits a rank defect for the degree 1 coefficients.

The degree 1 loading coefficients can be estimated when GPS station deformations are augmented in the joint inversion. Surface loading induced deformation at the i^{th} station can be written as (e.g. Kusche and Schrama 2005):

$$\begin{bmatrix}\delta h\\ \delta e\\ \delta n\end{bmatrix}_i = \frac{3ag\rho_w}{\rho_e}\sum_{n=1}^{N}\sum_{m=-n}^{n}\frac{1}{2n+1}\begin{bmatrix} h'_n\bar{Y}_{nm}(\theta_i,\lambda_i)\\ \frac{l'_n\partial\bar{Y}_{nm}(\theta_i,\lambda_i))}{\sin\theta\partial\lambda}\\ \frac{-l'_n\partial\bar{Y}_{nm}(\theta_i,\lambda_i))}{\partial\theta}\end{bmatrix}T_{nm} + \begin{bmatrix}\epsilon_h\\ \epsilon_e\\ \epsilon_n\end{bmatrix} \tag{4}$$

Here the local deformation is provided in the height, east and northward direction. The h'_n and l'_n load Love numbers convolve the surface load to the upward and lateral direction respectively. Since the GPS deformation is provided in the CM frame of the Earth we must use degree 1 load Love numbers which are transformed in this frame $h_1^{'CM} = h_1^{'CX} - 1 - k_1^{'CX}$, and $l_1^{'CM} = l_1^{'CX} - 1 - k_1^{'CX}$. Here 'CX' may indicate any of the isomorphic frames as described by Blewitt (2003).

In contrast to the GRACE observation equation, there is no rank defect for the degree 1 surface loading coefficients since $h_1^{'CM} \approx -1.3$ and $l_1^{'CM} \approx -0.9$ are non-zero. Furthermore, since these load Love numbers are not unity, there exists a degree 1 *deformation* which differs significantly from a pure *translation*. We exploit this fact by simultaneously fitting a 7 parameter Helmert transformation in the joint inversion every week. In that way, the degree 1 surface loading is estimated from the GPS network deformation, while the translation parameters are allowed to absorb residual nuisance signal related to the GPS processing (see also Rietbroek et al 2012b; Collilieux et al 2011). We do not simultaneously estimate the Helmert parameters in the GPS-only inversions as in those cases too much signal is absorbed by the Helmert parameters.

The ocean bottom pressure changes derived from virtually all ocean models, reflect the mass induced differences from an ocean at rest. However, time variations of the geoid also induce changes in the ocean bottom pressure, which are not captured by most of the models. The simulated OBP changes, expressed in equivalent water height, can therefore be represented as the sea surface height (ignoring steric effects) relative to the time-variable geoid height as caused by the same surface load:

$$\delta P(\theta,\lambda) = \Delta M_0 + a\sum_{n=1}^{N}\sum_{m=-n}^{n}\left(1-\frac{3\rho_w(1+k_n^{'})}{\rho_e(2n+1)}\right)\bar{Y}_{nm}(\theta,\lambda)T_{nm} + \epsilon_P \qquad (5)$$

The mass-correction parameter, ΔM_0, is constant over the ocean and is estimated every week in order to make the ocean model mass consistent with the estimated surface load.

3.1 Joint Inversion Scheme

We use the combination of GRACE, GPS and FESOM data as a reference solution. The proposed scheme differs in the following aspects from those used in Rietbroek et al (2009) and Rietbroek et al (2012b). Firstly, we use updated data, GRACE release 05 data, FESOM ocean bottom pressure from a more refined model setup, and GPS data with an improved processing and including a larger number of stations. Secondly, Rietbroek et al (2012b) loosely constrained station coordinates before transforming the normal equation systems in terms of surface loading coefficients and Helmert parameters. In this study, we fix the Earth orientation parameters for GPS to those used in the GRACE solution, and no additional coordinate constraints are applied before the transformation step. This actually increases the noise somewhat but we obtain a more consistent solution in terms of its reference frame. Thirdly, the weighting of the three different data types is now obtained from a variance component estimation (e.g. Koch and Kusche 2002). The square root of the estimated variance components varying over time is shown in Fig. 2. It is interesting to note that the variance component of FESOM shows an annual behavior, which suggest that the seasonal behavior may be somewhat over- or underestimated. Although we use a diagonal error-covariance for the FESOM data, we expect that significant error-covariances may be present. Such covariances would decrease the relative weight of the model in the inversion. To partially compensate for this effect, and to increase the relative weight of the true observations,

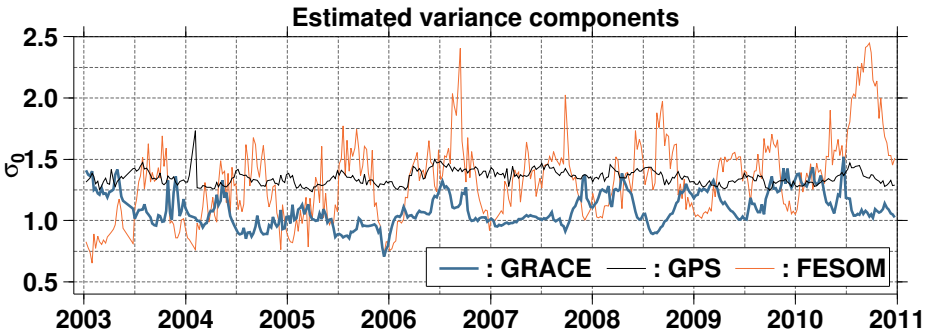

Fig. 2 Time varying behavior of the estimated variance components in the joint inversion. The factors represent the scaling of the formal errors of each data source.

we additionally rescale the FESOM error by a factor 5 after the optimal VCE factors have been obtained. A comparison of bottom pressure changes from the inversion with data from independent ocean bottom pressure recorders confirms that indeed a better correlation is obtained when rescaling the FESOM errors.

3.2 Regularization of the GPS Solution

In this paper, a special focus lies on the ability of GPS-network inversions to fill up a possible mission gap. An inversion for surface loading using Eq. 4 is possible for relatively low degrees. Here we choose a maximum truncation degree of 10, for the GPS-network solutions. An unconstrained solution poses no problem numerically, but the solution exhibits spurious oscillations in regions where there are few or no GPS stations (see Fig. 4). Blewitt and Clarke (2003) tackled this problem by forcing the solution in the ocean domain to a self-consistent sea level. This is an equipotential surface which is mass consistent with the terrestrial load. Alternatively, Kusche and Schrama (2005) applied a constraint which regularized the solution over the ocean towards zero.

Here, we propose a regularization technique which makes a compromize between the two methods. Instead of strictly enforcing an equipotential surface, we regularize the solution in the ocean domain towards it. The strength of the regularization can be tuned and therefore allows more flexibility when solving the systems. Physically, the regularization procedure may be interpreted as allowing the solution over the ocean to contain some dynamic topography.

When ignoring steric effects, the dynamic ocean topography, ΔT_{oce} can be seen as the difference of the dynamic ocean surface (i.e. $T(\theta,\lambda)$ and a time-variable equipotential sea surface $\tilde{S}$.

$$\Delta T_{oce}(\theta,\lambda) = O(\theta,\lambda)\left(T(\theta,\lambda) - \tilde{S}(\theta,\lambda)\right) \tag{6}$$

The difference on the right hand side is evaluated only in the ocean domain by multiplying it by the ocean function $O(\theta,\lambda)$.

In the following discussion, it is convenient to stack the spherical harmonic coefficients in row vectors (i.e. $\mathbf{t} = \begin{bmatrix} T_{00} \cdots T_{NN} \end{bmatrix}^T$). In the spectral domain, Eq. 6 can be written in matrix form (Rietbroek et al 2012a):

$$\Delta\mathbf{t}_{oce} = \mathbf{O}\left(\mathbf{t} - \tilde{\mathbf{s}}\right) \tag{7}$$

The matrix $\mathbf{O}$ operator and its complement $\mathbf{I} - \mathbf{O}$ map a spherical harmonic set of coefficients to the ocean or land domain respectively. The eigenvectors of the matrix are typically used in spatio-spectral concentration problems (Simons et al 2006). The self-consistent sea level, contained in $\tilde{\mathbf{s}}$, is by itself induced by changes in the land surface load, $\mathbf{t}_{land}$. It is computed by solving the sea level equation (going back as early as Woodward 1888), which can be written as a linear operator as well (Dahlen 1976; Rietbroek et al 2012a):

$$\tilde{\mathbf{s}} = \mathbf{G}_{SLE}\mathbf{t}_{land} = \mathbf{G}_{SLE}\left(\mathbf{I} - \mathbf{O}\right)\mathbf{t} \tag{8}$$

The matrix $\mathbf{G}_{SLE}$ can be obtained by solving:

$$\left(\mathbf{P} - \mathbf{G}_{N-U}\mathbf{O}\right)\mathbf{G}_{SLE} = \mathbf{G}_{N-U} \tag{9}$$

Where $\mathbf{P} = \mathrm{diag}\begin{bmatrix} 0\ 1 \cdots 1 \end{bmatrix}$ is a unit diagonal matrix with the degree zero entry set to 0. The diagonal matrix $\mathbf{G}_{N-U}$ is dependent on the load Love numbers and maps a surface load to the difference between the geoid (N) and the bottom deformation (U):

$$\mathbf{G}_{N-U} = \mathrm{diag}\left[1\ \frac{\rho_w}{\rho_e}\left(1 + k_1^{'} - h_1^{'}\right) \cdots\ \frac{3\rho_w}{(2n+1)\rho_e}\left(1 + k_n^{'} - h_n^{'}\right)\right] \tag{10}$$

The degree 0 values of the matrices are explicitly set to $\mathbf{P}(1,1) = 0$ and $\mathbf{G}_{N-U}(1,1) = 1$, which ensures that mass is conserved globally. The choice of the frame origin of the degree 1 load Love numbers is irrelevant as the combination $(1 + k_n^{'} - h_n^{'})$ is independent of the reference system (Blewitt 2003). Substituting Eq. 8 in Eq. 7 yields:

$$\Delta\mathbf{t}_{oce} = \mathbf{O}\left(\mathbf{I} - \mathbf{G}_{SLE}\left(\mathbf{I} - \mathbf{O}\right)\right)\mathbf{t} = \mathbf{F}\mathbf{t} \tag{11}$$

Eq. 11, can be viewed as a pseudo observation equation; adding a priori knowledge. Setting the expected value, $\mathrm{E}\{\Delta\mathbf{t}\} = 0$, and chosing a covariance matrix, $\mathbf{C}_{\Delta\mathbf{t}}$, we can construct a regularization term expressed in terms of the unknown surface loading coefficients:

$$\mathbf{\Psi}_{oce} = \alpha\mathbf{F}^T\mathbf{C}_{\Delta\mathbf{t}}^{-1}\mathbf{F} \tag{12}$$

Here, α, is an optional regularization parameter, with which one can tune the strength of the regularization. We approximate $\mathbf{C}_{\Delta\mathbf{t}}$ by first constructing an expected residual signal, consisting of output from the WaterGAP Global Hydrology Model (Döll et al 2003) which is augmented by the difference between the release 04 and release 05 dealiasing product. This residual is consequently mapped to the ocean domain using the $\mathbf{O}$ operator. As depicted by the signal degree variances in Fig. 3, this mapping operation removes a significant part of the simulated signal (i.e. the land component). A constant diagonal covariance matrix is then constructed by taking the RMS over the time domain 2002-2007, for each spherical harmonic coefficient. A regularization parameter, $\alpha = 100$, is additionally applied in order to obtain realistic surface loading results from a GPS inversion. This is shown exemplary for GPS week 1400 (5-11 Nov 2006), for which the GPS-I solution is shown in Fig. 4, and the associated degree variances are also plotted in Fig. 3.

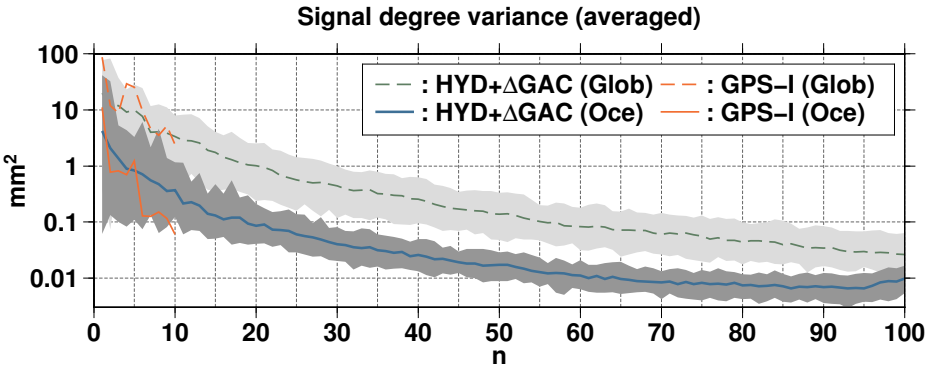

Fig. 3 Degree variance (averaged per coefficient) of a residual signal consisting of WGHM model data and the difference of the weekly RL04 and RL05 GAC products. The shaded area spans the variations over the time period from 2002-2007. The thicker lines denote the corresponding RMS. The lowering of curves is caused by the ocean operator **O**, which removes a significant amount of signal. Signal degree variances of the GPS-I solution for GPS week 1400 are shown in orange.

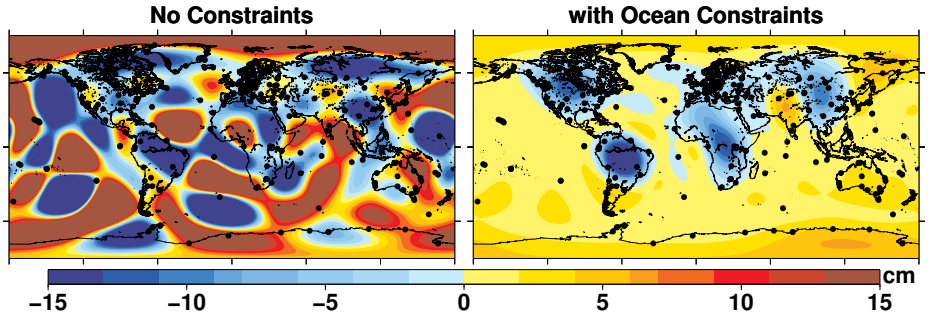

Fig. 4 Left: Unconstrained GPS solution up to degree and order 10, for the GPS week 1400 (5-11 Nov. 2006). Right: GPS solution where oceanic constraints are applied (GPS-I). GPS stations are indicated by black circles.

4 Filling GRACE Mission Gaps

We propose three methods to fill GRACE mission gaps. For the first method (GPS-I) no data outside the gap is needed. We perform a GPS inversion with the constraint from Sec. 3.2. This way, surface loading coefficients up to degree 10 are obtained. A temporal smoothing is applied by stacking 5 subsequent weekly normal equation systems in a running mean sense.

Unfortunately, the heterogeous coverage of the GPS network is very sensitive to spatial aliasing. The necessity to constrain the solution over the ocean is obvious from Fig. 4. However, even over land regions with a sparse station coverage, the signal may be either damped (when no stations exist in the region of maximum signal) or falsely amplified (when isolated stations are affected by strong local signals). The interplay often also results in a spatial shift of the maxima. Most of the loading signal shows a strong seasonal behavior, such that changes in the magnitude and phase are expected in regions with few GPS stations. The second

gap-filler method (GPS-C) tries to correct for these effect by applying correction parameters to the GPS-I solutions based on an overlapping period before (and optionally after) the mission gap. For this means, each surface loading coefficient in the GPS normal equation, with the regularization already applied, is expanded with a set of correction parameters consisting of a polynomial and an annual sinusoid:

$$T_{nm}^{GPS}(t) = T_{nm}^{*GPS}(t) + \sum_{i=0}^{p} T_{nm}^{(i)}(t - t_0)^i + T_{nm}^{c}\cos(\Omega t) + T_{nm}^{s}\sin(\Omega t) \qquad (13)$$

Obviously, this introduces additional rank defects in the weekly normal equation system. However, the correction parameters are not intended to be solved on the weekly level but are constrained by data from a longer overlapping period at the side(s) of the mission gap where both GRACE and GPS data exists. In the overlapping period, the coefficients $T_{nm}^{*GPS}(t)$, are fixed to the values as obtained from the reference solution and the correction parameters may be consequently estimated. Within the mission gap, the estimated correction parameters, which are independent on data in the gap itself, are now fixed to those as obtained above but the coefficients, $T_{nm}^{*GPS}(t)$ are now estimated every week.

In this study, we simulate two GRACE mission gaps. The first gap is the calendar year 2006. The overlapping period is chosen to be 3/4 year long at both sides of the gap. For this overlapping period, a polynomial up to degree 1 (bias and trend) is estimated as well as the annual cosine and sine amplitudes.

The second gap is about 1.5 year wide (centered at March 2010) but the correction parameters are estimated only from data before the mission gap (1.5 year overlapping period). For this gap, a bias and an annual sinusoid are estimated as nuisance parameters.

Due to the applied corrections, the seasonal behavior of the GPS-C gap-filler method is essentially determined by the reference solution itself. For comparison, we also construct a third gap-filler method (REF-S) which simply consists of a seasonal fit (and the same polynomial as in the nuisance parameters) to the coefficients of the joint inversion.

The chosen overlapping periods are kept relatively short to test whether a minimal amount of data suffice to make a gap-filler solution. Longer overlapping periods are also possible but are left out of the discussion.

5 Results

5.1 Surface Loading Coefficients

To assess the performance of the gap-filler methods, we compute approximate signal-to-noise ratios in the simulated mission gaps:

$$SNR_{nm} = \frac{\sum_{t_i \in gap}\left(T_{nm}^{REF}(t_i)\right)^2}{\sum_{t_i \in gap}\left(T_{nm}^{REF}(t_i) - T_{nm}^{gapfiller}(t_i)\right)^2} \qquad (14)$$

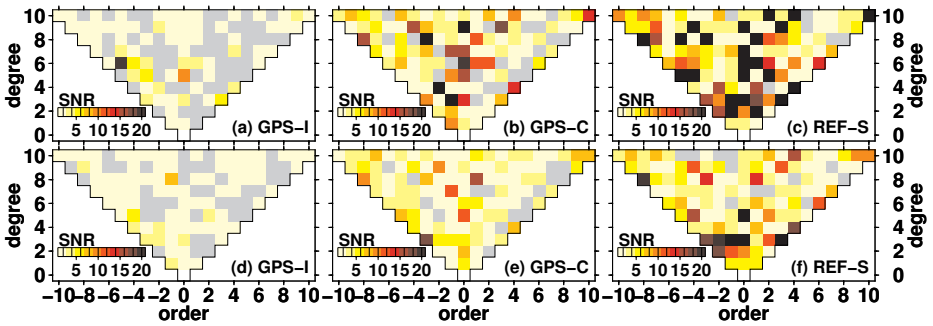

Fig. 5 Coefficient-wise signal to noise ratios of the three gap-filler methods (from left to right GPS-I, GPS-C and REF-S). The top and bottom row reflect the double sided and single sided gap respectively. SNR values below 0.8 are plotted in gray.

Where the signal is taken as that as obtained from the joint inversion, and the error is approximated as the difference between the reference and the gap-filler solution. If the gap-filler method performs well, SNR_{nm} is larger than 1. We plotted in Fig. 5 the signal-to-noise ratios for each of the two simulated gaps, and for all three gap-filler methods.

The uncorrected GPS-I inversion (left column of Fig. 5) shows a limited capability to reproduce the combination solution. Most of the surface loading coefficients have a noise level which is comparable or larger than that of the signal itself. The situation is improved for the GPS-C solution when correction parameters are applied (center column). The highest signal-to-noise ratios are in fact obtained by just filling the gap with a seasonal curve from the reference solution (REF-S). This suggests that, in terms of surface loading coefficients, the noise level of the (sub-annual) signal in the GPS-C solutions is larger than the difference between the signal and the seasonal gap-filler method.

The time variation of a selection of surface loading coefficients are plotted in Fig. 6. It is clear that for some coefficients, the uncorrected GPS-I solution (orange curve) wanders off from the combination solution. This is mostly the result of the spatial aliasing of the signal into the GPS solution. This effect has been the motivation to estimate and remove a correction curve from the data in an overlapping interval (shaded in lightgray). The corrected curves (in green), follow the coefficients from the combination solution more closely, although the significant differences can still be seen.

5.2 Selected Hydrological Basin Averages

Spherical harmonic coefficients of surface loading represent global averaged values. Since the GPS station network is very heterogeneous, it can be expected that the performance of a GPS-only solution is spatially dependent. We therefore compare the gap-filler methods in terms of basin averages for a variety of basins.

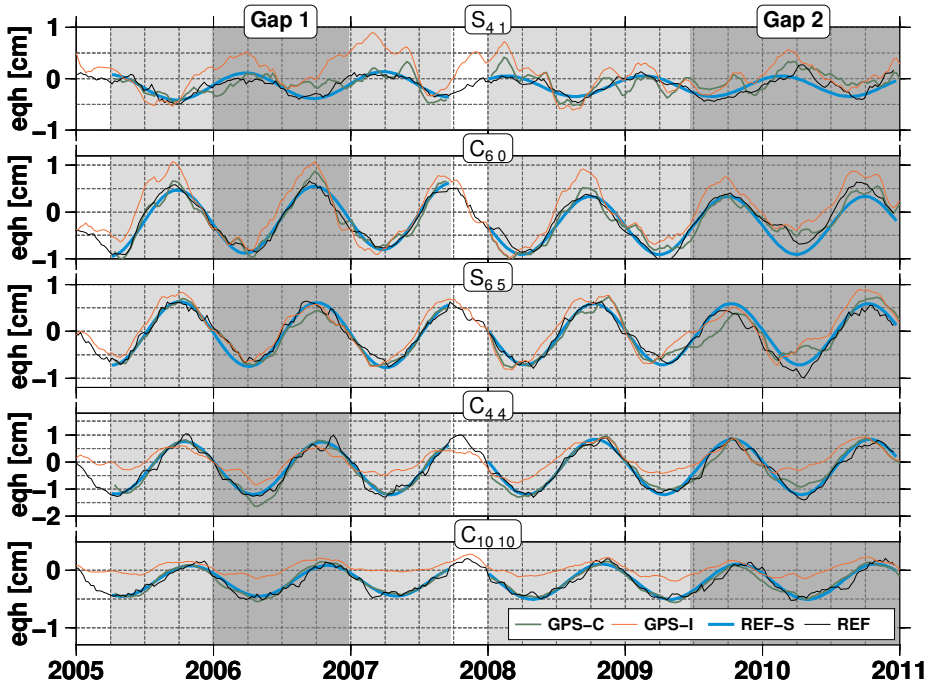

Fig. 6 Time variation of selected surface loading coefficients (combination and gap-filler solutions) expressed in equivalent water height (eqh). The simulated gaps and their corresponding overlapping periods are indicated by the dark and light shaded regions respectively.

In the spectral domain, the average surface load in a basin can be computed as (Wahr et al 1998):

$$\tilde{h}_\vartheta = \frac{f_\vartheta}{\vartheta_{00}} \sum_{n=0}^{N} \sum_{n=-m}^{m} \vartheta_{nm} w_n T_{nm} \tag{15}$$

Here, the spherical harmonic coefficients of the basin are denoted by ϑ_{nm}. Optionally, a set of filter coefficients, w_n, can be applied to reduce high frequency noise. We use here a 200 km Gaussian filter (Jekeli 1981), but this has only a minor effect for the truncation $N = 10$ we use.

Since the truncation degree is very low, the basin estimates are strongly influenced by leakage effects. These attenuate (leakage-out) or contaminate (leakage-in) the estimated signal of interest. To compensate for these effects, a scale factor, f_ϑ, is commonly applied (Velicogna and Wahr 2006; Fenoglio-Marc et al 2012; Baur et al 2009). Unfortunately, there is no unique way to compute this factor and several methods exist. Here, we introduce a new method to compute f_ϑ which accounts for the damping of the annual signal in hydrology. For this means, we took the WaterGap model (Döll et al 2003) and computed the annual sine and cosine amplitudes, $T_{nm}^{c/s,WG}$, in terms of surface loading coefficients. This annual signal is then filtered/truncated and, because of the linearity of the averaging operation,

Basin f_ϑ (Δt_a[doy])	Method	Gap$_1$ RMS	Gap$_1$ ΔRMS	Gap$_2$ RMS	Gap$_2$ ΔRMS	N_{stat}
Amazon	GPS-I	11.9	14.5	10.8	9.0	5
1.20 (2)	GPS-C	19.9	5.7	13.3	3.5	5
	REF-S	15.6	3.4	16.2	5.3	5
Orinoco	GPS-I	15.7	39.8	21.4	26.8	1
3.95 (-42)	GPS-C	34.7	7.1	32.6	15.3	1
	REF-S	35.2	10.4	36.9	23.7	1
Parana	GPS-I	6.1	2.9	5.9	4.6	9
0.90 (-9)	GPS-C	7.9	4.2	5.3	4.9	9
	REF-S	5.5	2.3	4.8	3.7	9
Zambezi	GPS-I	5.5	5.0	3.4	6.3	1
0.98 (-2)	GPS-C	8.3	2.5	7.1	2.6	1
	REF-S	7.6	1.6	8.2	2.1	1
Mississippi	GPS-I	3.4	3.4	5.2	3.3	6
1.15 (-7)	GPS-C	3.6	2.3	8.0	6.5	6
	REF-S	4.6	2.3	3.8	1.7	6
Ob	GPS-I	5.3	2.8	5.7	2.9	4
0.87 (3)	GPS-C	4.4	2.6	5.3	3.2	4
	REF-S	4.2	1.3	3.2	1.4	4
Ganges	GPS-I	10.8	4.6	12.7	7.4	0
1.51 (-9)	GPS-C	9.8	4.3	10.9	5.8	0
	REF-S	10.9	3.8	11.5	5.8	0
Danube	GPS-I	5.4	2.3	6.1	2.5	21
1.12 (-1)	GPS-C	3.8	2.1	4.3	3.0	21
	REF-S	4.0	1.7	4.6	2.7	21
Yukon	GPS-I	2.8	3.2	1.8	4.2	5
0.98 (3)	GPS-C	5.9	1.6	3.9	2.5	5
	REF-S	5.3	1.2	4.2	1.4	5

Table 1 Root mean squares of the three types of gap-filler solutions, and their residuals w.r.t. the combination solution (REF), in terms of basin averages. The scale factor and expected seaonal phase shift is given for each basin in the first column. All standard deviations are scaled with f_ϑ. The last column, contains the amount of GPS stations found within the region encompassing the basin and a surrounding buffer of 200 km.

a basin average can be obtained in terms of separate cosine and sine components:

$$\tilde{h}^c_\vartheta \cos(\Omega t) + \tilde{h}^s_\vartheta \sin(\Omega t) = \cos(\Omega t) \sum_{n=0}^{N} \sum_{n=-m}^{m} \vartheta_{nm} w_n T^{c,WG}_{nm} + \sin(\Omega t) \sum_{n=0}^{N} \sum_{n=-m}^{m} \vartheta_{nm} w_n T^{s,WG}_{nm} \tag{16}$$

The attenuation factor f_ϑ and phase shift, Δt_a of the annual signal is derived from comparing the unfiltered annual amplitude ($N = 100$ and no filter) with the filtered basin average ($N = 10$ and a 200 km Gaussian filter):

$$f_\vartheta = \sqrt{\frac{\bar{h}^{c2}_\vartheta + \bar{h}^{s2}_\vartheta}{\tilde{h}^{c2}_\vartheta + \tilde{h}^{s2}_\vartheta}}, \quad \Delta t_a = \frac{1}{\Omega}\left[\arctan\left(\frac{\tilde{h}^s_\vartheta}{\tilde{h}^c_\vartheta}\right) - \arctan\left(\frac{\bar{h}^s_\vartheta}{\bar{h}^c_\vartheta}\right)\right] \tag{17}$$

For a variety of basins, the damping factor and the associated phase shift are tabulated in Tab. 1. With the exception of the Orinoco basin, which is strongly influenced by the neighbouring Amazon, most of the basins have a damping factor that remains to within 20% of 1 and a phase shift of less than 10 days. The limited maximum truncation degree of 10 will cause a lot of the signal to leak out of the basin. At the same time however, we find that the leakage of signal into the basin

is of the same order of magnitude or even larger.

The RMS of the residuals, ΔRMS, in Table 1 provide rough estimates of weekly accuracies which are obtainable with the gap-filler methods. Since most of the hydrological signal follows a relatively smooth annual variation, the filling of the gap with a seasonal curve may already provide a good approach, although in some cases the GPS-C gap-filler solution works better (Amazon, second gap). On the level of spherical harmonic coefficients, we have seen that the GPS-C solutions improved virtually all of the coefficients compared to the GPS-I solution. In terms of basin averages, this can also be concluded for most basins. However, some in basins (first and 2nd gap of the Parana, 2nd gap of the Danube, Mississippi and Ob), the GPS-I solution outperforms the corrected series. Among all factors, a favourable GPS coverage in those regions may contribute to this.

The rescaled time variation of the basin averages are shown in Fig. 7. The plots confirms most of our findings from the previous paragraph, but additionally visualize that, during the second gap, the gap-filler solutions tend to diverge more strongly.

6 Conclusion and Discussion

We have assessed the ability of GPS-derived surface loading to fill the expected GRACE mission gap. As can be expected, the accuracy of the surface loading as obtained from GPS-only inversions is significantly less than that obtained by the GRACE mission. In terms of surface loading coefficients, we found that reducing a set of correction parameters from the GPS solutions increased the signal to noise ratios within the simulated gaps significantly. However the more simple seasonal gap-filler method (REF-S), where a seasonal curve is extended into the mission gap, outperforms the GPS gap-filler methods GPS-I and GPS-C in terms of residual RMS. This can be concluded from the time series of spherical harmonic surface loading coefficients and from time variations of almost all hydrologic basin averages considered. Although the REF-S gap-filler method fits the data very well, it should be noted that its use is restricted to the study of a simple harmonic seasonal variation and a trend. Although not shown here, we believe that the GPS-I and GPS-C may still offer useful information in the study of episodic or highly time-variable signal in dedicated regions, provided the signal is large enough and a good GPS station coverage exists.

The estimates in many basins benefit from the removal of the correction parameters from the GPS solution. However, in some basins (e.g. Mississippi, Danube, Parana) the uncorrected GPS solutions outperform the corrected ones, in particular in the second (one-sided) mission gap. The GPS-I and GPS-C solutions perform best in the Yukon and Danube basin, which may be due to a favourable GPS measurement geometry (i.e. densily distributed, or well placed GPS stations). However, as mentioned before, the seasonal gap-filler method appears to be less noisy.

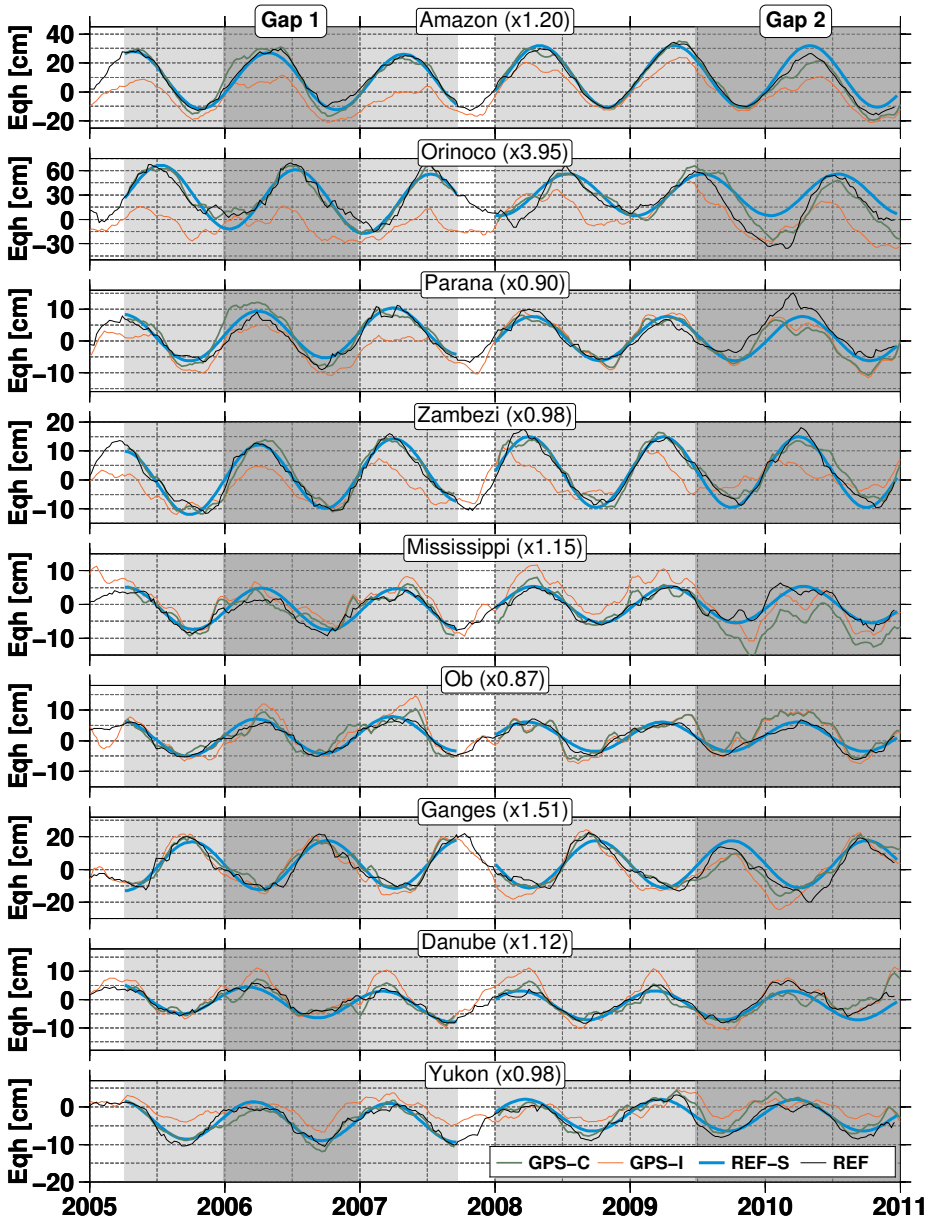

Fig. 7 Rescaled basin averages for selected hydrological basins, during the simulated mission gaps.

We suspect that one of the largest pitfalls of using GPS-derived surface loading solutions as a gap-filler lies in the spatial aliasing problem. The most obvious implication is the demonstrated necessity to apply a constraint over the ocean. But even over land there remain large areas where the solution is unconstrained by GPS stations. Unfortunately, this spatial aliasing problem is not expected to vanish when the time resolution is lowered, since the GPS network is not changing much over such periods. A further complication will be the retrieval of surface loading trends from GPS network changes. In the GPS-C solution, the secular changes are removed a priori from the stations and are then determined from the data in the overlap interval. However, when using only GPS network data, GPS orbit errors, and non-surface loading effects such as glacial isostatic adjustment and plate motion complicate the retrieval of surface loading trends (see for example Wu et al 2010).

Although limited in its use by itself, we do not doubt that the GPS network deformations contain valuable information on surface loading phenomena. In this line of reasoning, we see this study as a strong incentive to investigate future methods to reduce spatial aliasing. From our point of view, one of the most promising techniques is the combination of GPS with complementary datasets such as High-Low satellite-to-satellite tracking from for example SWARM, or with low degree variations of the gravity field from Satellite Laser Ranging.

Acknowledgements Financial support of this study has been provided by the German research foundation, under grants KU1207/6-3, DI473/41-3, FL592/1-3, SCHR779/4-3, in the framework of the special priority program: SPP1257 “mass transport and mass distribution in the system Earth”. We would like to thank the German Space Operations Center (GSOC) of the German Aerospace Center (DLR) for providing continuously and nearly 100% of the raw telemetry data of the twin GRACE satellites. The helpful suggestions of Xiaoping Wu and an anonymous reviewer were highly appreciated.

References

Baur O, Kuhn M, Featherstone W (2009) Grace-derived ice-mass variations over greenland by accounting for leakage effects. Journal of Geophysical Research: Solid Earth (1978–2012) 114(B6)

Blewitt G (2003) Self-consistency in reference frames, geocenter definition, and surface loading of the solid earth. Journal of Geophysical Research 108(B2):2103

Blewitt G, Clarke P (2003) Inversion of earth’s changing shape to weigh sea level in static equilibrium with surface mass redistribution. Journal of Geophysical Research (Solid Earth) 108:2311, DOI 10.1029/2002JB002290

Blewitt G, Lavallée D, Clarke P, Nurutdinov K (2001) A new global mode of earth deformation: seasonal cycle detected. Science 294(5550):2342–5, DOI 10.1126/science.1065328

Chambers DP, Schröter J (2011) Measuring ocean mass variability from satellite gravimetry. Journal of Geodynamics 52(5):333–343

Collilieux X, van Dam T, Ray J, Coulot D, Métivier L, Altamimi Z (2011) Strategies to mitigate aliasing of loading signals while estimating gps frame parameters. Journal of Geodesy pp 1–14

Dahle C, Flechtner F, Gruber C, König D, König R, Michalak G, Neumayer K (2013) GFZ GRACE Level-2 Processing Standards Document for Level-2 Product Release 0005. Scientific Technical Report STR12/02 - Data Revised Edition (January 2013)

Dahlen FA (1976) The passive influence of the oceans upon the rotation of the earth. Geophysical Journal of the Royal Astronomical Society 46(2):363–406

Desai SD (2002) Observing the pole tide with satellite altimetry. Journal of Geophysical Research 107(C11):3186, DOI 10.1029/2001JC001224
Döll P, Kaspar F, Lehner B (2003) A global hydrological model for deriving water availability indicators: model tuning and validation. Journal of Hydrology 270(1-2):105–134
Dziewonski A (1981) Preliminary reference earth model. Physics of The Earth and Planetary Interiors 25(4):297, DOI 10.1016/0031-9201(81)90046-7
Eicker A, Schumacher M, Kusche J, Döll P, Müller-Schmied H (2014) Calibration/data assimilation approach for integrating GRACE data into the WaterGAP Global Hydrology Model (WGHM) using an ensemble Kalman filter . Surveys in Geophysics (submitted)
Fenoglio-Marc L, Rietbroek R, Grayek S, Becker M, Kusche J, Stanev E (2012) Water mass variation in the mediterranean and black sea. Journal of Geodynamics 59-60(0):168 – 182, DOI 10.1016/j.jog.2012.04.001, Mass Transport and Mass Distribution in the System Earth
Flechtner F, Morton P, Watkins M, Webb F (2013) Status of the grace follow-on mission. In: Proc. IAG Symposia, Gravity, Geoid and Height Systems (GGHS2012), Venice, Italy (accepted)
Fritsche M, Dietrich R, Knöfel C, Rülke A, Vey S, Rothacher M, Steigenberger P (2005) Impact of higher-order ionospheric terms on gps estimates. Geophysical Research Letters 32(23):L23,311
Jekeli C (1981) Alternative methods to smooth the Earth's gravity field. The Ohio State University
Koch KR, Kusche J (2002) Regularization of geopotential determination from satellite data by variance components. Journal of Geodesy 76(5):259–268
Köhl A, Siegismund F, Stammer D (2012) Impact of assimilating bottom pressure anomalies from grace on ocean circulation estimates. Journal of Geophysical Research: Oceans (1978–2012) 117(C4)
Kusche J (2003) A monte-carlo technique for weight estimation in satellite geodesy. Journal of Geodesy 76(11):641–652
Kusche J, Schrama EJO (2005) Surface mass redistribution inversion from global gps deformation and gravity recovery and climate experiment (grace) gravity data. Journal of Geophysical Research (Solid Earth) 110(B9):9409, DOI 10.1029/2004JB003556
Pilinski E, Nerem R (2011) Experiments with eof-based gravity field reconstructions using slr and grace data. In: AGU Fall Meeting Abstracts, vol 1, p 0884
Rietbroek R, Brunnabend SE, Dahle C, Kusche J, Flechtner F, Schröter J, Timmermann R (2009) Changes in total ocean mass derived from grace, gps, and ocean modeling with weekly resolution. Journal Of Geophysical Research-Oceans 114(C11004):C11,004, DOI 10.1029/2009JC005449
Rietbroek R, Brunnabend SE, Kusche J, Schröter J (2012a) Resolving sea level contributions by identifying fingerprints in time-variable gravity and altimetry. Journal of Geodynamics 59:72–81, DOI DOI: 10.1016/j.jog.2011.06.007
Rietbroek R, Fritsche M, Brunnabend SE, Daras I, Kusche J, Schröter J, Flechtner F, Dietrich R (2012b) Global surface mass from a new combination of grace, modelled obp and reprocessed gps data. Journal of Geodynamics 59-60(0):64 – 71, DOI 10.1016/j.jog.2011.02.003, Mass Transport and Mass Distribution in the System Earth
Rignot E, Velicogna I, Van den Broeke M, Monaghan A, Lenaerts J (2011) Acceleration of the contribution of the greenland and antarctic ice sheets to sea level rise. Geophysical Research Letters 38(5)
Schmidt R, Flechtner F, Meyer U, Neumayer KH, Dahle C, König R, Kusche J (2008) Hydrological signals observed by the grace satellites. Surveys in Geophysics 29(4-5):319, DOI 10.1007/s10712-008-9033-3
Sheard B, Heinzel G, Danzmann K, Shaddock D, Klipstein W, Folkner W (2012) Intersatellite laser ranging instrument for the grace follow-on mission. Journal of Geodesy 86(12):1083–1095
Simons FJ, Dahlen FA, Wieczorek MA (2006) Spatiospectral concentration on a sphere. SIAM Rev 48(3):504–536, DOI http://dx.doi.org/10.1137/S0036144504445765
Steigenberger P, Rothacher M, Dietrich R, Fritsche M, Rülke A, Vey S (2006) Reprocessing of a global gps network. Journal of Geophysical Research 111(B5):B05,402
Tapley BD, Bettadpur S, Ries JC, Thompson PF, Watkins MM (2004) Grace measurements of mass variability in the earth system. Science 305:503–506, DOI 10.1126/science.1099192
Timmermann R, Danilov S, Schröter J, Böning C, Sidorenko D, Rollenhagen K (2009) Ocean circulation and sea ice distribution in a finite element global sea ice-ocean model. Ocean

Modelling 27(3-4):114–129, DOI 10.1016/j.ocemod.2008.10.009,
Velicogna I, Wahr J (2006) Acceleration of greenland ice mass loss in spring 2004. Nature 443(7109):329–331, DOI 10.1038/nature05168
Wahr J, Molenaar M, Bryan F (1998) Time variability of the earth's gravity field: Hydrological and oceanic effects and their possible detection using grace. Journal of Geophysical Research 103:30,205–30,230, DOI 10.1029/98JB02844
Wang X, Gerlach C, Rummel R (2012) Time-variable gravity field from satellite constellations using the energy integral. Geophysical Journal International 190(3):1507–1525
Woodward R (1888) On the form and position of mean sea level. Geological Survey Bulletin 48:87–170
Wu X, Heflin MB, Ivins ER, Fukumori I (2006) Seasonal and interannual global surface mass variations from multisatellite geodetic data. Journal of Geophysical Research (Solid Earth) 111(B10):9401, DOI 10.1029/2005JB004100
Wu X, Heflin MB, Schotman H, Vermeersen BLA, Dong D, Gross RS, Ivins ER, Moore AW, Owen SE (2010) Simultaneous estimation of global present-day water transport and glacial isostatic adjustment. Nature Geoscience 3(9):642, DOI 10.1038/ngeo938
Wu X, Ray J, van Dam T (2012) Geocenter motion and its geodetic and geophysical implications. Journal of Geodynamics 58:44–61
Zaitchik BF, Rodell M, Reichle RH (2008) Assimilation of grace terrestrial water storage data into a land surface model: Results for the mississippi river basin. Journal of Hydrometeorology 9(3):535–548